Inflammation
https://doi.org/10.1007/s10753-024-02074-7

RESEARCH

OTUD1 Deficiency Alleviates LPS-Induced Acute Lung Injury in Mice by Reducing Inflammatory Response

Weiwei Zhu[1,2] · Qianhui Zhang[1] · Leiming Jin[1] · Shuaijie Lou[1] · Jiaxi Ye[1] · Yaqian Cui[1] · Yongqiang Xiong[2] · Mengsha Lin[1] · Guang Liang[1,2,3] · Wu Luo[1,2] · Zaishou Zhuang[1]

Received: 1 April 2024 / Revised: 5 May 2024 / Accepted: 3 June 2024

Abstract

The ovarian tumor (OTU) family consists of deubiquitinating enzymes thought to play a crucial role in immunity. Acute lung injury (ALI) and acute respiratory distress syndrome (ARDS) pose substantial clinical challenges due to severe respiratory complications and high mortality resulting from uncontrolled inflammation. Despite this, no study has explored the potential link between the OTU family and ALI/ARDS. Using publicly available high-throughput data, 14 OTUs were screened in a simulating bacteria- or LPS-induced ALI model. Subsequently, gene knockout mice and transcriptome sequencing were employed to explore the roles and mechanisms of the selected OTUs in ALI. Our screen identified OTUD1 in the OTU family as a deubiquitinase highly related to ALI. In the LPS-induced ALI model, deficiency of OTUD1 significantly ameliorated pulmonary edema, reduced permeability damage, and decreased lung immunocyte infiltration. Furthermore, RNA-seq analysis revealed that OTUD1 deficiency inhibited key pathways, including the IFN-γ/STAT1 and TNF-α/NF-κB axes, ultimately mitigating the severity of immune responses in ALI. In summary, our study highlights OTUD1 as a critical immunomodulatory factor in acute inflammation. These findings suggest that targeting OTUD1 could hold promise for the development of novel treatments against ALI/ARDS.

KEY WORDS OTUD1 · inflammation · acute lung injury · STAT1 · NF-κB

Abbreviations

ALI	Acute lung injury
OTUD1	OTU domain containing 1
LPS	Lipopolysaccharide
BALF	Bronchoalveolar lavage fluid
GAPDH	Glyceraldehyde-3-phosphate dehydrogenase
STAT1	Signal transducer and activator of transcription 1
TNF-α	Tumor necrosis factor α
IL-6	Interleukin 6
NF-κB	Nuclear factor kappa-B
IκB-α	Inhibitor of κBα

Weiwei Zhu, Qianhui Zhang and Leiming Jin are Contributed equally.

✉ Guang Liang
wzmcliangguang@163.com

✉ Wu Luo
wuluo@wmu.edu.cn

✉ Zaishou Zhuang
zhuang372@163.com

[1] Affiliated Cangnan Hospital and Chemical Biology Research Center, Wenzhou Medical University, Wenzhou 325000, China

[2] Department of Cardiology and Medical Research Center, the First Affiliated Hospital of Wenzhou Medical University, Wenzhou 325000, China

[3] School of Pharmaceutical Sciences, Hangzhou Medical College, Hangzhou 311399, China

Introduction

Acute lung injury (ALI) is an acute inflammatory lung condition that can progress to severe acute respiratory distress syndrome (ARDS) [1]. It arises from a series of direct (pulmonary) or indirect (extrapulmonary) lung injuries, such as pneumonia or non-pulmonary sepsis, characterized by excessive, uncontrolled inflammation, and apoptosis [2, 3]. The pathophysiological features of ALI/ARDS include alveolar barrier dysfunction, heightened inflammation, and pulmonary edema [4]. Although existing treatments for ALI have been shown to improve dysfunction, the mortality rate in ALI patients remains high, underscoring the need

Published online: 22 July 2024

for further understanding of the underlying mechanisms of ALI and the identification of novel targets [5].

Excessive immune responses are recognized as a primary factor in the pathogenesis of ALI/ARDS. During the initial pulmonary infection, pathogen-associated molecular patterns (PAMPs) or endogenous damage-associated molecular patterns (DAMPs) attract and activate resident alveolar macrophages (AM) via pattern recognition receptors (PRRs) like Toll-like receptors (TLRs) [6, 7]. This activation prompts the release of pro-inflammatory mediators and chemokines by the AM, facilitating the infiltration of leukocytes, particularly neutrophils and monocytic cells, into the alveolar sacs [8]. The persistence of invading pathogens or diseased tissues keeps both resident and infiltrating immunocytes in a state of constant activation, culminating in an uncontrolled inflammatory response known as a "cytokine storm" [9]. Several classical inflammatory pathways, including the nuclear factor-κB (NF-κB) pathway, MAPK pathway, STAT pathway, and NLRP3 inflammasome pathway, have been identified as contributors to the initiation and progression of ALI/ARDS [10]. Within these pathways, several key mediators have been identified, and corresponding inhibitors have been discovered or designed and shown potential therapeutic effects in ALI mouse models. However, various limitations of these inhibitors have hindered their clinical application. Thus, focused exploration of additional regulatory proteins to identify more potential targets is expected to reveal novel therapeutic strategies for ALI/ARDS.

Ubiquitination is a crucial post-translational modification process that intricately controls various biological functions, including inflammatory response [11]. Deubiquitinating enzymes (DUBs) remove ubiquitin molecules from substrate proteins and play a pivotal regulatory role in immune responses by deubiquitinating key proteins associated with inflammation and immunity [12]. Within the DUB superfamily, the ovarian tumor (OTU) family is a classical subset consisting of sixteen members [13]. Several OTUs have been studied to understand their functions in modulating inflammatory responses across different diseases. For instance, OTUB1 has shown efficacy in alleviating chronic hepatitis [14]; OTUD1 exhibits inhibition of chronic inflammatory bowel disease [15]; and OTULIN has been reported to prevent skin inflammation [16]. Despite these recognitions, the exact role of OTUs in acute pneumonia and ALI remains elusive.

In this study, we investigated potential regulatory OTUs and their involvement in ALI development. Bioinformatic analysis of several high-throughput RNA-seq datasets from ALI samples revealed that OTUD1 is highly associated with ALI and was selected for further study. The role of OTUD1 in ALI was validated using whole-body OTUD1 knockout mice, while transcriptome sequencing elucidated the underlying mechanisms. These comprehensive studies shed light on the significant impact of OTUD1 in acute lung inflammation, presenting OTUD1 as a promising novel target for ALI treatment.

Materials and Methods

Antibodies and General Reagents

Lipopolysaccharide (LPS from E. coli; Cat# L2630) were purchased from Sigma-Aldrich (St. Louis, MO, USA). Antibody against OTUD1 (Cat# orb185712) was purchased from Biorbyt (Cambridge, UK). Antibodies against IκB-α (Cat# sc-1643), JAK2 (Cat# AF6022) and phosphor-JAK2 (Cat# AF3024) were purchased from Santa Cruz Biotechnology (Dallas, TX, USA). Antibodies for phospho-NF-κB p65 (Cat# 3033), and NF-κB p65 (Cat# 8242) were purchased from Cell Signalling Technology (Danvers, MA, USA). Antibodies against Lamin B (Cat# ab133741) were purchased from Abcam (Cambridge, UK). GAPDH antibody (Cat# AB-P-R001) was purchased from Hangzhou Goodhere Biotechnology (Hangzhou, China). STAT1 antibody (Cat# AG3318) and phosphor-STAT1 (Cat# AF5935) antibody were purchased from Beyotime (Shanghai, China). Fluorophore-labeled antibodies including PE-anti-F4/80 (Cat# 123110), APC-anti-CD11b (Cat# 101212), PerCP-anti-Ly6G (Cat# 127654), and FITC-anti-CD45 (Cat# 103108) were purchased from BioLegend (San Diego, CA, USA). Horseradish peroxidase-conjugated goat anti-mouse IgG (Cat# A0192) and goat anti-rabbit IgG (Cat# A0208) were purchased from Beyotime. Hematoxylin and eosin (H&E) staining kit (Cat# G1120) were purchased from Solarbio Life Sciences (Beijing, China).

Animal Experiments

All animal care and experimental procedures were approved by the Animal Policy and Welfare Committee of the Wenzhou Medical University (Wenzhou, Zhejiang, China; approval number: wydw2020-0012). OTUD1 knockout ($OTUD1^{-/-}$; Supplementary Figure S1) male mice and the littermate wide-type mice on a C57BL/6J background were provided by Dr. Fuping You (Peking University Health Science Center, Beijing, China) [17]. The viability and proper development of $OTUD1^{-/-}$ mice were normal during the experiments. All animals were housed in a pathogen-free room at 22℃ ± 2℃, 50% – 60% humidity, 12 h: 12 h light/dark cycle and fed with a standard rodent diet and water that was available ad libitum. The animals were acclimatized to the laboratory for 2 weeks before initiating the studies. All animal experiments were performed and analysed by blinded researchers. The mice were divided randomly into groups and housed in the microisolator cages with 6 mice

per cage. Each mouse was assigned a temporary random number within the weight range and then given a permanent numerical designation in the cages. For each group, one cage was randomly selected from the pool of all cages.

Male C57BL/6 J wildtype (WT) mice were randomly divided into two groups: (1) mice treated with vehicle control (WT-CON), (2) mice treated with LPS (WT-LPS). Similarly, male OTUD1$^{-/-}$ mice were divided into two groups: (1) mice treated with vehicle control (KO-CON), (2) mice treated with LPS (KO-LPS). ALI was induced essentially as described previously [18]. Briefly, mice were anesthetized with 2% sodium pentobarbital (80 mg·kg^{-1}, i.p., Sigma-Aldrich). Heart rate, body temperature, and toe pinch were monitored to detect the depth of anesthesia. Mice were then challenged by intratracheal injection of LPS (5 mg·kg-1; dissolved in 0.9% saline) or 0.9% saline alone. At 6 h post-LPS challenge, mice were sacrificed and bronchoalveolar lavage fluid (BALF) was collected by perfusing with 2 × 200 µL PBS solution through the tracheal cannula. Blood and lung tissue samples were collected for subsequent analyses.

Collected BALF samples were centrifuged at 3000 rpm for 5 min. The supernatant was used for determining total protein levels and levels of cytokines using ELISA. Cell pellets were resuspended in 100 µL 0.9% saline, and the total cell counts were determined with a hemocytometer. Neutrophil count was acquired by counting 200 cells on a smear prepared by Wright–Giemsa staining (Nanjing Jiancheng Bioengineering Institute; Nanjing, Jiangsu, China). Lung wet/dry weights were determined as an index of pulmonary edema. The right middle lobes were collected, and wet weights were recorded. Tissues were heated in a thermostatically controlled oven at 65 °C for 24 h, and dry weights were measured.

Survival Analysis in Sepsis Model

E.coli strain DH5α was grown in Luria Broth (LB) media and the density was determined at 600 nm (OD600) using NanoDrop2000. The corresponding colony-forming units (CFUs) were determined on LB agar plates. Viable *E. coli* DH5α (1×10^9 CFU per mice) in 0.5 mL PBS was injected into the peritoneal cavity (i.p.). Survival of the mice was monitored every 6 h for 3 days.

Lung Histology

Lung tissues were fixed in 4% paraformaldehyde, embedded in paraffin and sectioned to a thickness of 5 µm. For routine histology, the sections were stained with haematoxylin and eosin. The lung injury scores (0–1) were determined by pathologist in blind manner using the criteria in previous report and shown in Supplementary Table S1 [19].

Immunostaining was performed on deparaffinized and hydrated lung sections. Antigen retrieval was performed by heating sections in sodium citrate buffer (pH 6.0). Sections were blocked in 1% bovine serum albumin (BSA; Sigma-Aldrich) in PBS for 30 min and incubated with primary antibody (1:100) overnight at 4 °C. Horseradish peroxidase (HRP)-labeled secondary antibodies were applied for 1 h at 37 °C. Immunoreactivity was detected by diaminobenzidine (DAB). Sections were counterstained with hematoxylin. Images were captured using a brightfield microscope. Image J analysis software version 1.53i (NIH; Bethesda, MD, USA) was used to calculate immunoreactivity.

Myeloperoxidase Activity Assay

Neutrophil tissue infiltration was evaluated in terms of myeloperoxidase (MPO) activity in lung tissue samples using an MPO Detection Kit (Nanjing Jiancheng Bioengineering Institute). Lung tissues were homogenized in 1 ml of 50 mM potassium PBS (pH 6.0) containing 0.5% hexadecyltrimethylammonium hydroxide and centrifuged at 15,000 g, 4℃ for 20 min. Ten microliters of the supernatant was transferred into PBS (pH 6.0) containing 0.17 mg·ml^{-1} 3,3'-dimethoxybenzidine and 0.0005% H_2O_2. MPO activity in the supernatant was determined by measuring the absorbance at 460 nm. Total protein levels were measured using a Pierce BCA Protein Assay Kit (Cat# 23225; Thermo Fisher). Data are presented as U·g^{-1} tissue.

Western Blot

Total protein and nuclear proteins from cells and lung tissues were extracted using lysis buffer (Boster Biological Technology; Pleasanton, CA, USA) and nuclear extraction kit (Beyotime), respectively. The protein concentration was measured and then the protein lysates were separated by 10% sodium dodecyl sulfate–polyacrylamide gel electrophoresis (SDS-PAGE) and transferred to polyvinylidene fluoride membranes. Membranes were blocked in Tris-buffered saline (pH 7.4, containing 0.05% Tween 20 and 5% non-fat milk) for 1.5 h at room temperature before incubating with primary antibodies at 4 ℃ overnight. Secondary antibodies were applied for 1 h at room temperature. Immunoreactivity was visualized using enhanced chemiluminescence reagent (Bio-Rad; Hercules, CA, USA) and quantified using Image J analysis software version 1.53i. Values were normalized to respective housekeeping proteins.

Transcriptome Sequencing

Total RNA from the tissues was isolated and purified using TRIzol reagent (Invitro-gen, CA, USA) following the manufacturer's procedure. The RNA amount and purity

of each lung sample were quantified using NanoDrop ND-1000 (NanoDrop; DE, USA). The RNA integrity was determined using Bioanalyzer 2100 (Agilent, CA, USA), and confirmed by electrophoresis with denaturing agarose gel. Poly (A) RNA is purified from 1 μg total RNA using Dynabeads Oligo (dT) 25–61005 (Thermo Fisher). Then the poly(A) RNA was fragmented into small pieces using Magnesium RNA Fragmentation Module (NEB, Cat. e6150, MA, USA). The cleaved RNA fragments were then reverse transcribed into cDNA by SuperScript™ II Reverse Transcriptase (Invitrogen). Finally, the sequence analysis was performed on an Illumina Novaseq™ 6000 following the manufacturer's instructions. After generating the final transcriptome, the expression levels of all transcripts were estimated. The differentially expressed mRNAs were selected with adj. p-value < 0.05.

For studies in Fig. 1, the public accessed transcriptome data in LPS-treated or gram-negative bacterial-infected mice lung were retrieved from the Gene Expression Omnibus database (www.ncbi.nlm.nih.gov/geo). Four series of database, GSE233206 [20], GSE214249, GSE104214, and GSE199546 [21] were selected. The raw count or FPKM were analysed by using Limma package to identifying differential expression genes.

ELISA Assay for Cytokines

Selected cytokines were detected in the mouse serum and BALF samples. Total protein was determined for normalization. Commercially available mouse TNF-α and IL-6 ELISA kits (MultiScience; Hangzhou, China) were used for these studies. Absorbance was measured at 450 nm using a SpectraMax® M5 Multi-Mode Microplate Reader (Molecular Devices; San Jose, CA, USA).

Flow Cytometry

Cell pellets prepared from BALF were resuspended in 100 μL FACS buffer (PBS with 2% FBS and 1 mM EDTA). Cells were stained with FITC-anti-CD45, PE-anti-F4/80, APC-anti-CD11b, and PerCP-anti-Ly6G for 30 min on ice. Cells were then washed three times with FACS buffer and detected using BD Accuri™ C6 Cytometer (BD Biosciences; Franklin Lakes, NJ, USA). Total viable single cells were first gated for CD45-positive immune cells and analyzed for F4/80, CD11b, and Ly6G. Neutrophils were presented as $CD11b^{+}$-$Ly6G^{+}$ and macrophages as $CD11b^{+}$-$F4/80^{+}$.

Real-Time qPCR

Total RNA was extracted from tissues using Trizol Reagent (Cat# 9109; Takara; Tokyo, Japan). RNA was reverse-transcribed using PrimeScript™ RT reagent (Cat# RR047A; Takara). Real-time PCR was conducted using TB Green® Premix Ex Taq™ II (Cat#RR820A; Takara) on CFX96 Touch Real-Time PCR Detection System (Bio-Rad). Relative expression was normalized to *Actb*. Target gene sequences are listed in Supplementary Table S2.

Statistical Analysis

All data are reported as Mean ± SEM. Statistical analysis was performed with GraphPad Prism 8.0 software (San Diego, CA, USA). We used one-way ANOVA followed by Dunnett's post hoc test when comparing more than two groups of data. P value less than 0.05 was considered to be statistically significant. Post-tests were run only if F achieved $P < 0.05$ and there was no significant variance inhomogeneity.

Results

Down-Regulation of OTUD1 Was Associated with Immune Responses to ALI

To determine the correlation between the OTU family and ALI, we screened 14 typical OTUs in lung samples infected with gram-negative bacteria (GSE233206) or treated with LPS, a characteristic pathogen component located in the outer membrane of gram-negative bacteria (GSE214249). Of these, *Otud1* (encoding the OTUD1 protein) and *Tnfaip3* (encoding the A20 protein) showed consistent decreases and increases in expression in both ALI models, respectively (Fig. 1A-B). This consistent pattern implied that they are potential correlates in ALI occurrence. Given that the role of A20 in LPS-induced inflammatory responses has been elucidated [22, 23], our focus shifted to OTUD1. The assessment was further validated in two additional ALI transcriptome sequencing databases (GSE104214 and GSE199546) with a decreasing trend of *Otud1* mRNA levels over time (Fig. 1C-D). Particularly, correlation analysis revealed a strong correlation between *Otud1* expression and the prototypical pro-inflammatory factor *Il1b*, underscoring the involvement of OTUD1 in the immune process (Fig. 1E). In addition, independent assessments of *Otud1* mRNA content and OTUD1 protein levels in LPS-treated ALI model lungs showed a consistent reduction of both (Fig. 1F-H). Taken together, these findings strongly indicated the relationship between OTUD1 and ALI.

OTUD1 Deficiency Prevented Tissue Damage in LPS- or Bacterial-Infected Lungs

To clarify the role of OTUD1 in ALI, we modeled ALI via exogenous LPS injection using OTUD1 knockout mice and

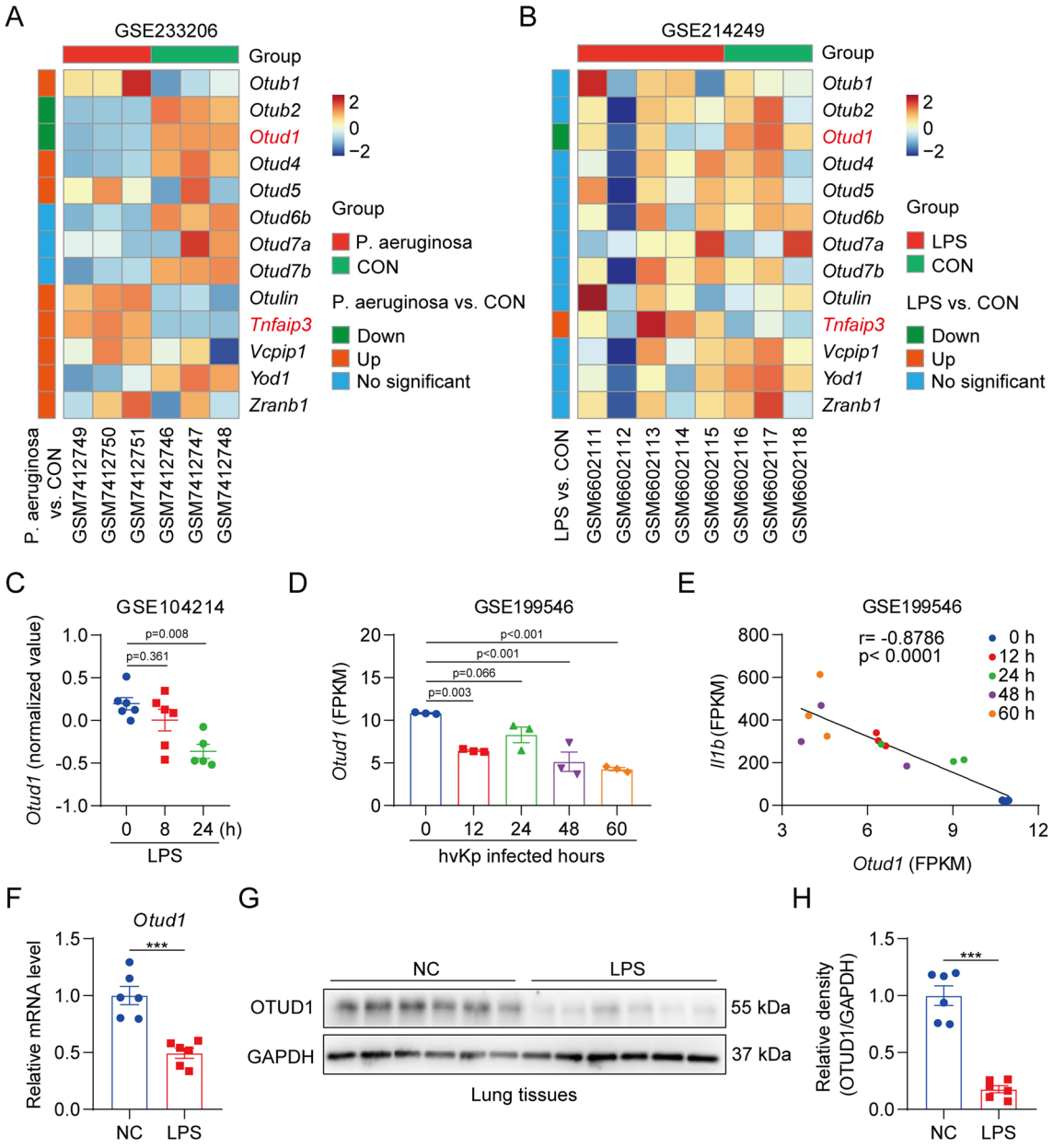

Fig. 1 Identification of the relativity between OTUD1 and acute lung injury (**A**-**B**) Heat map showing the expression level of 14 OTUs in GSE233206 (**A**) and GSE214249 (**B**) datasets, respectively. *Otud1* and *Tnfaip3* were marked red due to its consistent trend in above datasets. (**C**) Transcription level of *Otud1* in GSE104214 dataset. (**D**) Transcription level of *Otud1* in GSE199546 dataset. (**E**) Pearson correlation analyses between the expression level of *Il1b* and *Otud1* in GSE199546 dataset. (**F**) The mRNA level of *Otud1* in lung tissues treated with/without LPS challenge. (**G**) OTUD1 protein levels in lung tissue treated with/without LPS challenge. (**H**) The densitometric quantification data of panel G. Data are represented as mean ± SEM; *$p < 0.05$; **$p < 0.01$; ***$p < 0.001$.

WT mice. Our results showed that LPS injection resulted in an increase in bronchoalveolar lavage fluid (BALF) protein concentration, indicating abnormal pulmonary vasculature permeability. Notably, OTUD1 deficiency significantly ameliorated this condition, as evidenced by a decrease in protein concentration (Fig. 2A). Additionally, parameters such as lung wet-to-dry ratio and histopathological damage, such as pulmonary edema, leukocytic infiltration, and increased alveolar wall thickness, were elevated in response to LPS stimulation. However, upon LPS injection, the KO-LPS group failed to exhibit the same level of induction as WT-LPS mice (Fig. 2B-D). Furthermore, *E. coli* is a gram-negative bacterium that induces systemic sepsis, which has similarities to LPS-induced ALI. To assess the effect of OTUD1 deletion under live bacterial infection, we monitored the mortality of mice infected with *E. coli*. Strikingly, all WT

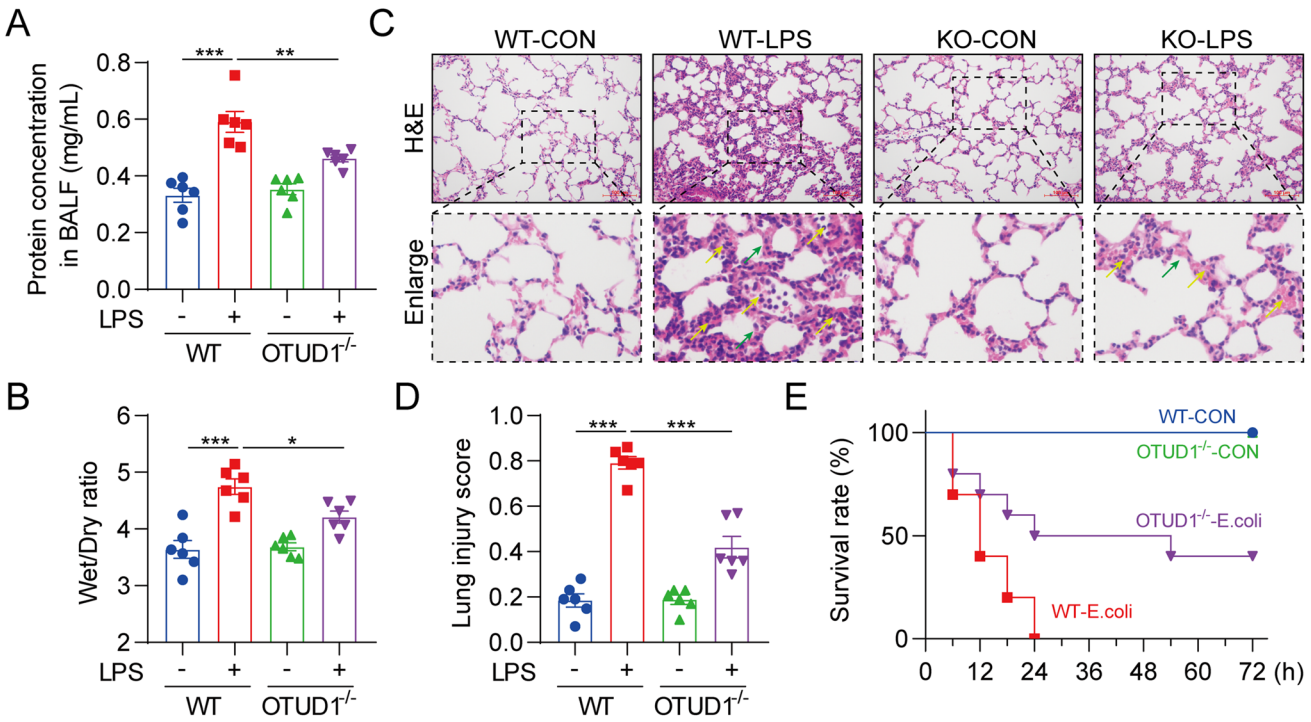

Fig. 2 OTUD1 knockout improves the lung injury under LPS or bacterial infection. C57BL/6 and OTUD1 knockout mice were challenged with intratracheal LPS (5 mg·kg^{-1}) for 6 h, to generate a lung injury model. **A** Total proteins in BALF samples were measured. **B** Lung wet/dry ratio. **C** Representative H&E-stained images of lung tissues. [scale bar = 100 μm]. Yellow arrows represented immunocytes infiltration, and green arrows showed alveolar septal thickening. **D** Quantification of lung injury scores. **E** Survival curve of WT and OTUD1$^{-/-}$ mice in a model of sepsis treated with a viable *E.coli* DH5α ($1 \times 10.^{9}$ CFU/mice, i.p.). Data are represented as mean ± SEM; n = 6 per group; *$p < 0.05$; **$p < 0.01$; ***$p < 0.001$.

mice succumbed within 24 h of *E.coli* infection, whereas the survival rate of OTUD1 knockout mice exceeded 40% (Fig. 2E). Taken together, all the profound difference underscored the protective role of OTUD1 deficiency in attenuating inflammation-induced injury.

OTUD1 Deficiency Mitigated LPS-Induced Immunocyte Infiltration in the Injured Lung

Immunocyte infiltration is not only one of the hallmarks of ALI but also an amplifying factor in its development, triggering an uncontrollable inflammatory response. Consistent with this, we observed a 3- to fourfold increase in cell numbers in BALF post-LPS stimulation, which notably improved when OTUD1 was deficient in mice (Fig. 3A). Furthermore, adhesion molecules such as *Vcam1* and *Icam1*, pivotal for cell localization following recruitment, showed increased expression under LPS treatment but suppressed transcription levels in the OTUD1 knockout group (Fig. 3B). Measurements of myeloperoxidase (MPO) activity in the lungs and nuclear staining further confirmed that LPS-induced recruitment of neutrophils was alleviated following OTUD1 deletion (Fig. 3C-D). Moreover, cellular staining using either macrophage markers (F4/80^{+}-CD11b^{+}) or neutrophil markers (Ly6G^{+}-CD11b^{+}) revealed a substantial reduction in LPS-induced influx of both macrophages and neutrophils in the absence of OTUD1 (Fig. 3E-H, Supplementary Figure S2). Finally, we quantified two typical pro-inflammatory factors, IL-6 and TNF-α, in serum and BALF. The results showed that OTUD1 knockout significantly reduced the secretion of these cytokines (Fig. 3I-J). These findings strongly suggested that the knockout of OTUD1 effectively prevents LPS-induced lung inflammation and improves lung injury.

OTUD1 Deficiency Blocked Multiple Inflammatory Pathways in the Lung

To reveal the mechanism by which OTUD1 deficiency has a protective effect against LPS-induced inflammation to ameliorate ALI, we conducted RNA-sequencing of lung tissues from the WT-LPS and KO-LPS groups. Principal component analysis (PCA) plots showed the consistency of the data within groups, as well as a distinct separation between the WT-LPS and KO-LPS groups (Fig. 4A). Subsequently, 9,394 differentially expressed genes (7,650 up-regulated and 1,744 down-regulated) were identified when comparing the sequencing data from KO-LPS to

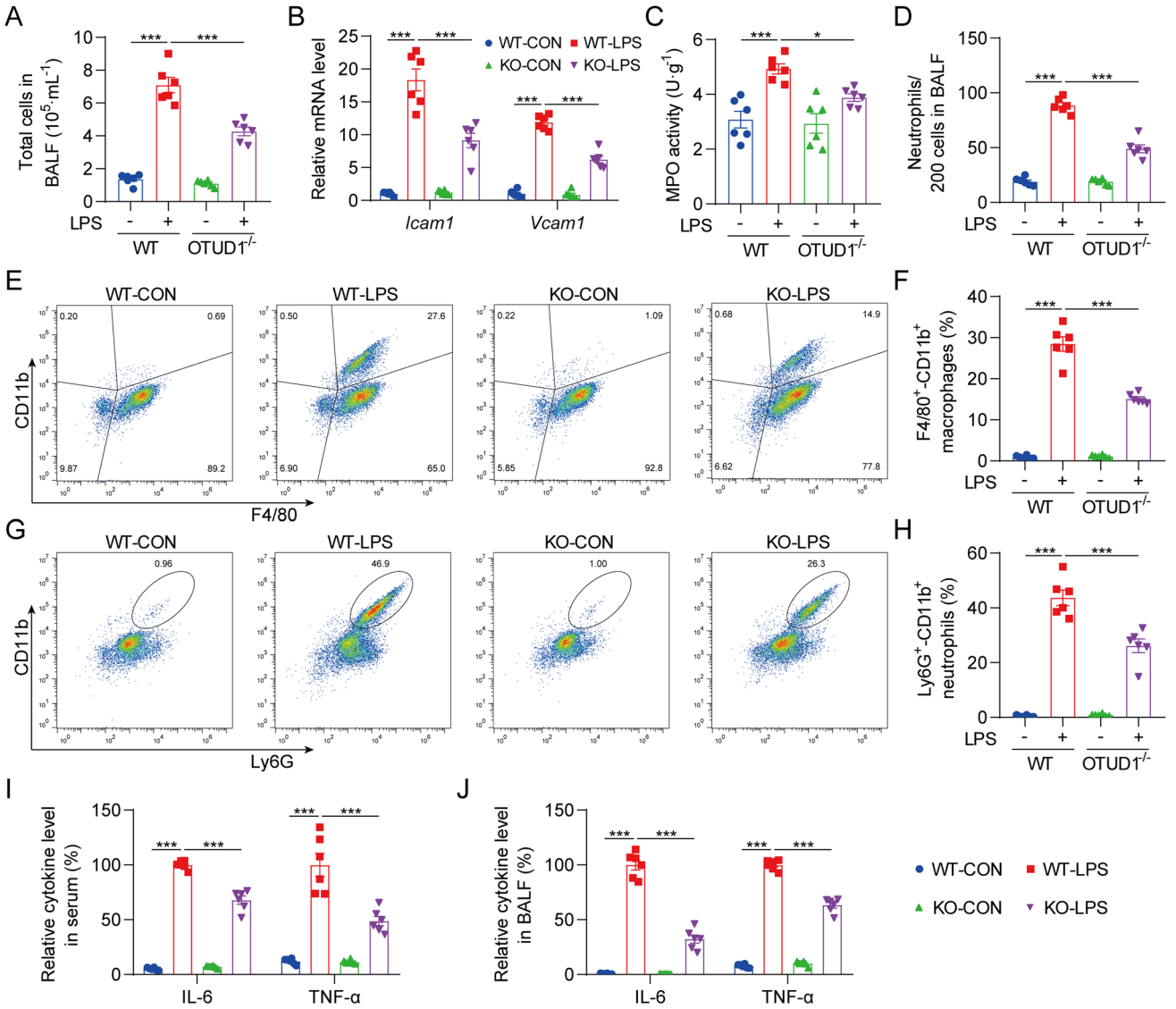

Fig. 3 OTUD1 knockout alleviates the immunocytes infiltration in injured lungs (**A**) Total cell counts in BALF samples measured by hemocytometer. (**B**) The mRNA levels of *Icam1* and *Vcam1* were detected by RT-qPCR in the lung tissues. (**C**) MPO activity level in lung lysates. (**D**) Neutrophils as assessed by Wright-Giemsa staining. (**E**–**H**) Flow cytometric detection of infiltrating cell populations in BALF samples. Representative flow dot plots are shown in panels E and G. CD11b$^+$-F4/80$^+$ represent monocyte-derived macrophages and CD11b$^+$-Ly6G.$^+$ represent neutrophils. (**F**) Quantification of macrophages and neutrophils monocyte is shown in panels F and H, respectively. (**I**-**J**) Levels of IL-6 and TNF-α in serum (**I**) and BALF samples (**J**) in mice challenged with/without LPS. Data are represented as mean ± SEM; n = 6 per group; *$p < 0.05$; **$p < 0.01$; ***$p < 0.001$.

WT-LPS (Fig. 4B). For these 1,744 down-regulated genes, gene enrichment analyses pinpointed several inflammatory features, specifically interferon-gamma (IFN-γ) responses, TNF-α signaling via NF-κB, and IL-6/JAK/STAT3 signaling (Fig. 4C). Moreover, predictions of transcription factors highlighted the dominance of signal transducer and activator of transcription 1 (STAT1), a key player in the IFN-γ pathway, and NF-κB in response to OTUD1 knockout (Fig. 4D). These coherent findings from gene enrichment and transcription factor prediction emphasized that OTUD1 deficiency affects IFN-γ responses and NF-κB activation. Furthermore, detailed expression analysis of the gene clusters involved in these pathways confirmed that they are repressed in the absence of OTUD1 (Fig. 4E-F).

We also performed gene enrichment and transcription factor prediction of genes up-regulated after OTUD1 deletion. Interestingly, our analysis mainly highlighted hallmarks associated with cell proliferation and migration, including epithelial-mesenchymal transition, apical junction, adipogenesis, and myogenesis (Supplementary

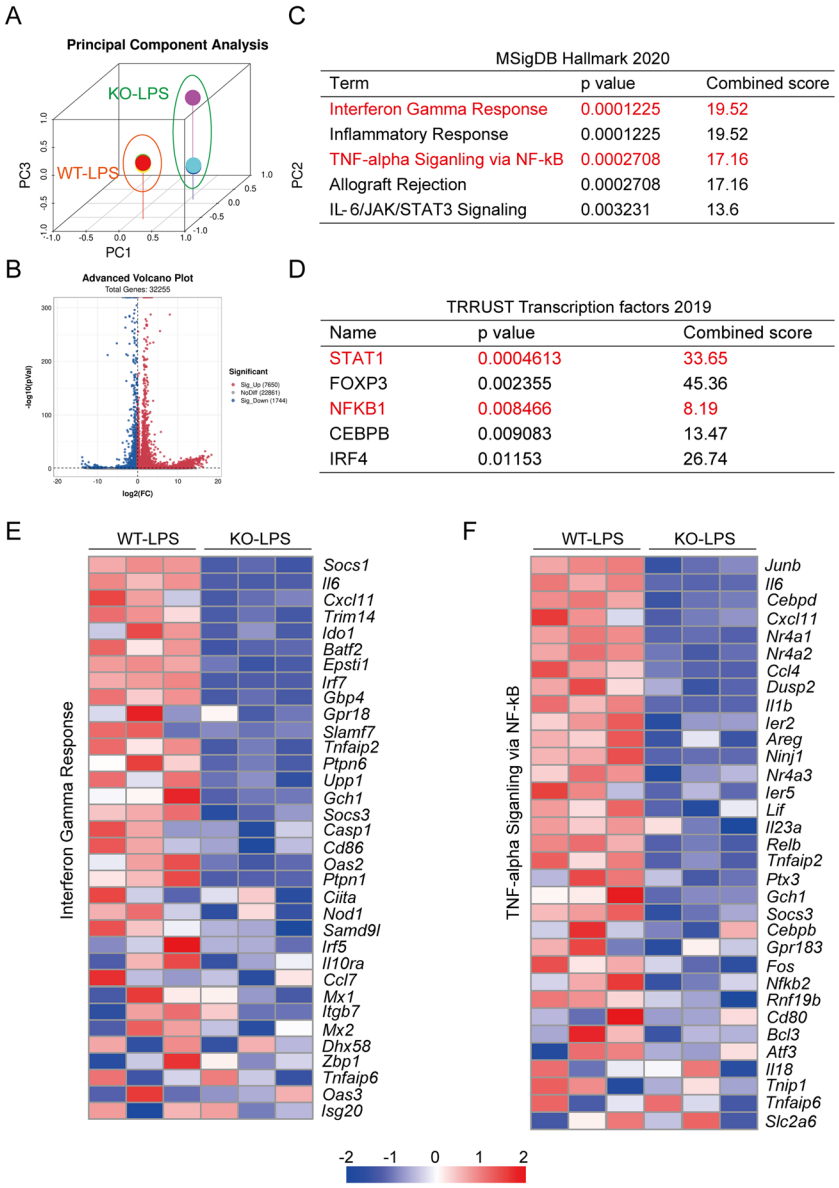

Fig. 4 RNA-seq analysis in WT and OTUD1 knockout mice both treated with LPS (**A**) Principal component analysis (PCA) of RNA-sequencing data in different lung samples. (**B**) Volcano plot analysis of transcriptional changes in KO-LPS compared to WT-LPS. The adj.p value threshold was set as ≤ 0.05. Red dots indicate upregulated genes, blue dots indicate downregulated genes, and gray dots indicate non-differentially expressed genes. (**C**) A comprehensive gene set enrichment analysis for the down-regulated genes was performed using MSigDB Hallmark 2020. (**D**) Transcription factor analysis of down-regulated genes through TRRUST Transcription factors 2019. (**E–F**) Heatmap showing the alternation of gene clusters in Interferon Gamma Response (**E**) and TNF-α Signaling via NF-κB (**F**) between WT-LPS and KO-LPS group.

Figure S3A). Intriguingly, the involvement of predicted transcription factors in regulating inflammation was minimal (Supplementary Figure S3B).

Comprehensive analysis of both down- and up-regulated genes in the absence of OTUD1 reconfirmed that OTUD1 deficiency impedes multiple inflammatory pathways, contributing to the amelioration of pulmonary inflammation in ALI.

OTUD1 Deficiency Prevented IFN-γ/STAT1-Induced Inflammatory Responses

IFN-γ is a key pro-inflammatory factor induced by LPS treatment that triggers a secondary inflammatory response upon secretion. The specific mechanism involves binding of IFN-γ to its receptor, leading to phosphorylation of JAKs and STAT1. Subsequently, phosphorylated STAT1 translocated into the nucleus and activated the transcription of IFN-γ-stimulated genes (ISGs), such as *Isg15*, *Cox2*, and *Ccl5* (Fig. 5A). To verify the regulatory role of OTUD1 deletion on the IFN-γ response, we initially assessed the phosphorylation levels of JAK2 and STAT1, revealing a significant decrease in the KO-LPS group (Fig. 5B-C). Furthermore, through immunoblotting and immunofluorescent staining, we confirmed a concomitant decrease in STAT1 translocation in LPS-treated lungs in the absence of OTUD1 (Fig. 5D-F). These alterations resulted in a consistent reduction in the transcription of ISGs including *Isg15*, *Cox2*, and *Ccl5* (Fig. 5G). Collectively, these findings affirmed that OTUD1 deficiency effectively impedes the IFN-γ/STAT1 signaling pathway.

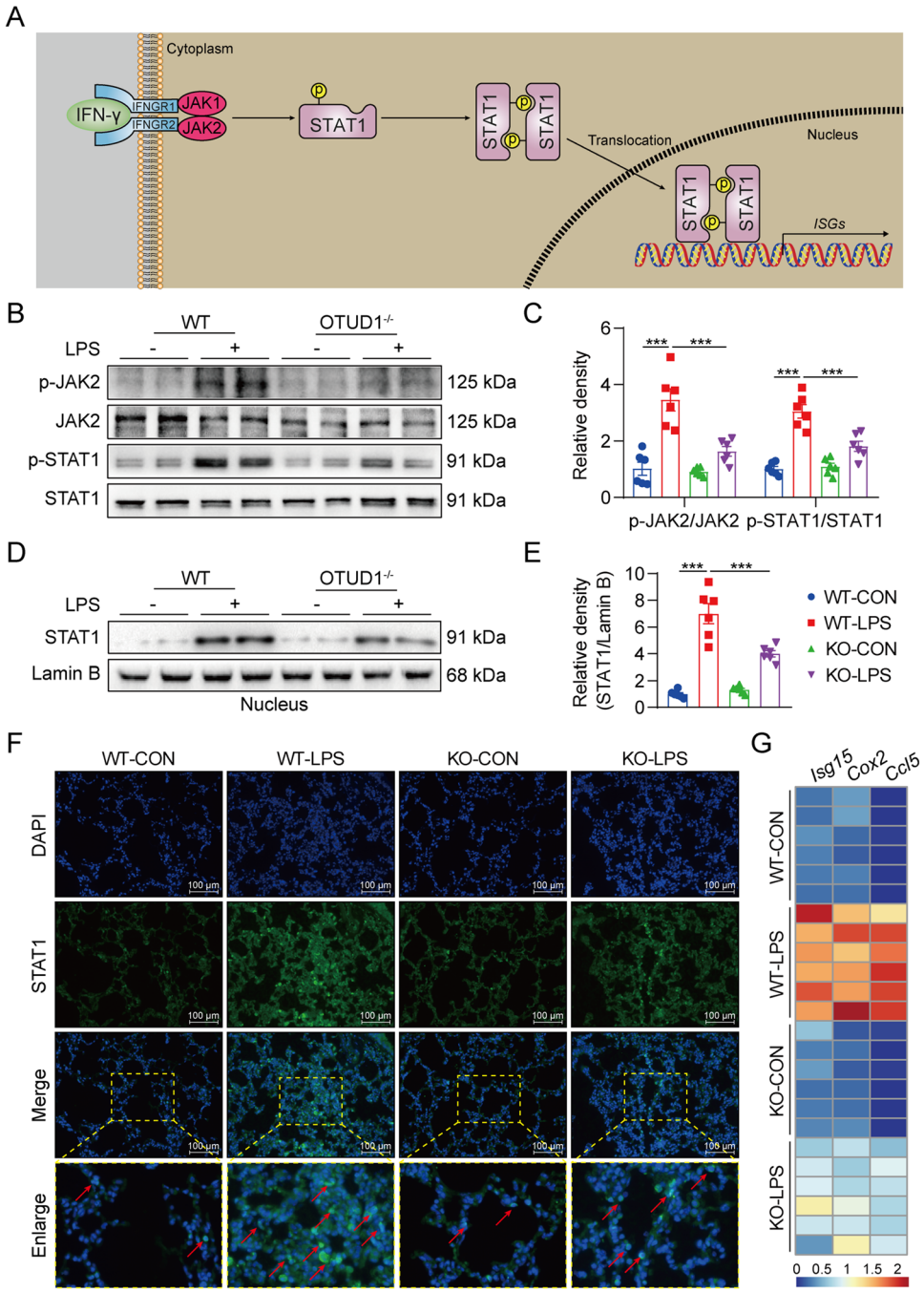

Fig. 5 OTUD1 knockout block the IFN-γ-STAT1 pathway (A) Schematic showing the IFN-γ-STAT1 signalling pathway. (**B**-**C**) Representative western blot analysis (**B**) and quantification (**C**) of p-JAK2 and p-STAT1 levels in lung tissue lysates. JAK2 and STAT1 was used as a loading control. (**D**-**E**) Representative western blot analysis (**D**) and quantification (**E**) of STAT1 levels in nuclear. Lamin B was used as a loading control. (**F**) Immunofluorescence staining for the STAT1 (green) in lung tissues [scale bar = 100 μm]. Cells were counterstained with DAPI (blue). (**G**) Heatmap showing the mRNA level of *Isg15*, *Cox2*, and *Ccl5* in lung tissues. Data are represented as mean ± SEM; n = 6 per group; *$p < 0.05$; **$p < 0.01$; ***$p < 0.001$.

OTUD1 Deficiency Suppressed LPS-Induced Activation of TNF-α Signaling through Inhibition of NF-κB

Similarly, TNF-α, another pro-inflammatory factor triggered by LPS treatment, initiated a secondary inflammatory response by binding to its receptor and activating the NF-κB element, leading to the transcription of various pro-inflammatory cytokines, including *Il1b*, *Il6*, *Tnf*, *Ccl2*, *Csf1*, and *Il12a* (Fig. 6A). To confirm the regulatory effect of OTUD1 deletion on NF-κB activation, we assessed the degradation of NF-κB inhibitor α (IκB-α) as well as the phosphorylation levels of p65 and STAT1, both of which were significantly reduced in the KO-LPS group (Fig. 6B-C). Additionally, immunoblotting and immunofluorescent staining revealed parallel changes in p65 translocation in LPS-treated lungs (Fig. 6D-F), showing a consistent reduction in the transcription of *Ccl2*, *Csf1*, and *Il12a* (Fig. 6G). These findings confirmed that OTUD1 deficiency effectively impedes the LPS-induced NF-κB signaling pathway.

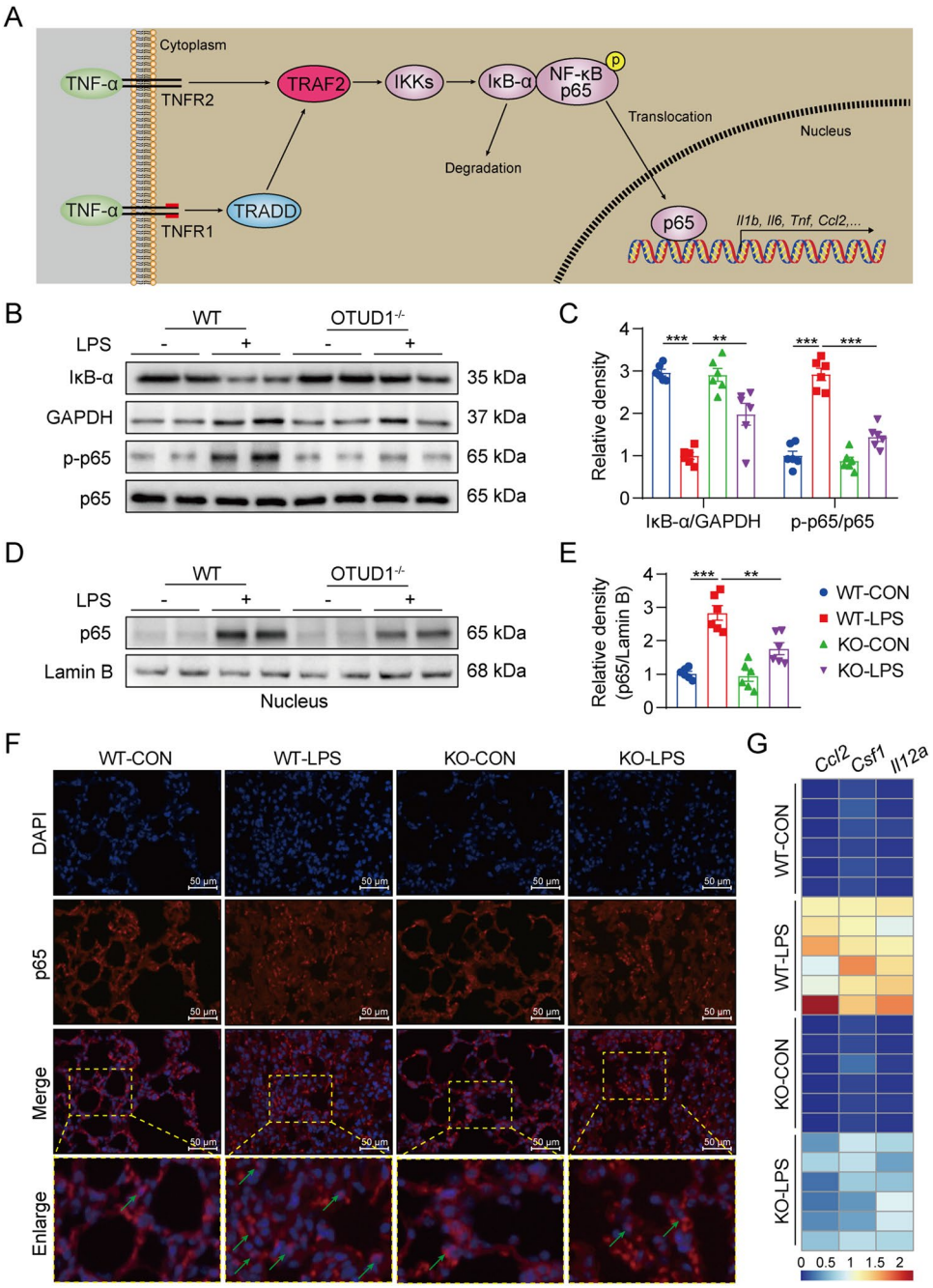

Fig. 6 OTUD1 knockout block the NF-κB pathway (**A**) Schematic showing the TNF-α signalling pathway via NF-κB activation. (**B**-**C**) Representative western blot analysis (**B**) and quantification (**C**) of IκB-α and p-p65 levels in lung tissue lysates. GAPDH and p65 was used as a loading control. (**D**-**E**) Representative western blot analysis (**D**) and quantification (**E**) of p65 levels in nuclear. Lamin B was used as a loading control. (**F**) Immunofluorescence staining for the p65 (red) in lung tissues [scale bar = 50 μm]. Cells were counterstained with DAPI (blue). (**G**) Heatmap showing the mRNA level of *Ccl2*, *Csf1*, and *Il12a* in lung tissues. Data are represented as mean ± SEM; n = 6 per group; *$p < 0.05$; **$p < 0.01$; ***$p < 0.001$.

Discussion

Our study focused on identifying a novel therapeutic target within the OTU family and delving into its mechanisms for the treatment of ALI. Through analysis of publicly available high-throughput data, knockout mouse modeling, and transcriptome sequencing, we observed three key results: (i) OTUD1 expression was reduced in ALI and negatively correlated with inflammatory levels; (ii) OTUD1 deficiency ameliorated ALI-associated pathological changes; (iii) OTUD1 deficiency effectively inhibited the IFN-γ response and NF-κB activation, thereby attenuating acute pneumonia in ALI. Overall, these findings strongly suggested that targeting OTUD1 could represent a promising immunosuppressive approach for the treatment of ALI.

OTUD1 was selected for this study because of the notable changes in its expression observed in lung infections caused by bacteria or LPS, especially in non-cancerous lung diseases that have been previously understudied. Previous studies have underscored the importance of OTUD1, identifying its involvement in DNA damage response, cell cycle regulation, and immune signaling pathways [24–26]. In the

realm of inflammatory-related diseases, OTUD1 plays a variety of roles: attenuating colonic inflammation in inflammatory bowel disease [15], maintaining immune balance in autoimmune conditions such as rheumatoid arthritis [27], and mitigating cerebral ischemic injury through inhibition of RIP2-mediated inflammation [28], among others. These findings highlighted the dual nature of OTUD1 as both an enhancer and repressor of inflammation in various diseases and organs. This dual characterization increases the complexity of understanding the role of OTUD1 in ALI.

Given that OTUD1 is a deubiquitinating enzyme, it would be intriguing to investigate whether the ubiquitination of the proposed downstream targets is affected by OTUD1. Our RNA-seq results revealed alterations in both the STAT1 and NF-κB pathways, suggesting that OTUD1 may not have a singular target responsible for the immune response in ALI. This observation is partly consistent with previous findings by *Chen* et al., who reported that OTUD1 targets CARD9 to activate NF-κB elements, a mechanism potentially relevant to ALI [29]. Additionally, although there are no direct reports demonstrating a relationship between OTUD1 and the STAT1 pathway, our previous research demonstrated that OTUD1 targets signal transducer and activator of transcription 3 (STAT3) to induce cardiac inflammation [30]. Therefore, we hypothesize that OTUD1 might also directly target STAT1, based on the similarities between STAT1 and STAT3.

Our preliminary analysis of publicly available sequencing data revealed a negative correlation between *Otud1* expression and the inflammatory marker *Il1b*, suggesting an immunosuppressive role of OTUD1 in ALI. Surprisingly, OTUD1 deficiency in LPS-treated mice reduced inflammatory response and improved ALI. This unexpected finding indicated that OTUD1 is compensatorily suppressed under inflammatory conditions, revealing its role as an immunopotentiator. Lung transcriptome sequencing supported this regulatory mechanism of OTUD1 expression, illustrating its involvement in the second phase of acute pneumonia. Our gene enrichment and transcription factor prediction further confirmed that cytokine-induced inflammatory responses (such as IFN-γ, TNF-α, and IL-6 pathways) were blocked in OTUD1 deficiency but not the TLR4 pathways, signifying OTUD1's participation in the later stages of ALI.

Moreover, Karlsson M et al. detected OTUD1 in various lung cell types, including B cells, mast cells, macrophages, pneumocytes, and epithelial cells using single-cell atlas analyses [31]. Sequencing data showed that OTUD1 knockout promotes tumor progression through epithelial-mesenchymal transition, highlighting the need for more targeted studies on the cell-specific functions of OTUD1. This targeted research approach aligns with our plans and promises to better understand OTUD1's precise role in lung biology and diseases.

The development of inhibitors targeting the enzymatic activity of DUBs like OTUD1 is a pivotal step in facilitating their clinical progression. Although no inhibitors specifically targeting OTUs have been reported, insights have been gained from the development of the ubiquitin-specific peptidase (USP) family of inhibitors. Several inhibitors, including b-AP15 and VLX1570, have been clinically tested against different members of the USP family [32, 33]. To identify potential inhibitors for OTUD1, screening methods similar to those used for USP inhibitors could be employed. Screening for USP inhibitors typically involves the use of detectable molecular markers introduced at the C-terminal of ubiquitin, such as Ub-AMC [34], Ub-rhodamine-110 [35], and Ub-PLA_2 [36]. The use of these conjugates in combination with active OTUD1 recombinant proteins in a catalytic assay could streamline the screening process to identify potential OTUD1 inhibitors in the future.

Conclusion

In conclusion, our study provides compelling evidence that OTUD1, identified from the OTU family, plays a crucial role in regulating the inflammatory response associated with ALI. OTUD1 deficiency disrupts multiple pro-inflammatory pathways, specifically affecting the IFN-γ/STAT1 and TNF-α/NF-κB axes, which ultimately ameliorates the pathological changes observed in ALI and improves the survival of sepsis patients. Hence, targeting OTUD1 emerges as a promising avenue for developing novel therapies for ALI/ARDS.

Supplementary Information The online version contains supplementary material available at https://doi.org/10.1007/s10753-024-02074-7.

Acknowledgements We thank Dr. Fuping You (Peking University Health Science Center, Beijing, China) for providing the OTUD1 knockout mice. We thank Scientific Research Center of Wenzhou Medical University for consultation and instrument availability that supported this work.

Authors' contributions Zaishou Zhuang, Wu Luo, and Guang Liang contributed to the literature search and study design. Weiwei Zhu, Qianhui Zhang, Leiming Jin, Shuaijie Lou, Jiaxi Ye, Yaqian Cui, Yongqiang Xiong, and Mengsha Lin performed the experiments. Weiwei Zhu and Qianhui Zhang contributed to data collection and analysis. Zaishou Zhuang and Wu Luo participated in the drafting of the article. Guang Liang and Wu Luo revised the manuscript.

Funding This study was supported by the National Key Research Project (2017YFA0506000 to G.L.), National Natural Science Foundation of China (21961142009 to G.L.), Postdoctoral Fellowship Program of CPSF (GZC20231957 to W.Z), Medical and Health Research Project of Zhejiang Province (2022KY348 to W.Z.), Zhejiang Provincial Key Scientific Project (2021C03041 to G.L.), and Wenzhou Science and Technology Key Project (2018ZY009 to G.L.).

Data Availability The data that support the findings of this study are available from the corresponding author upon reasonable request. Some data may not be made available because of privacy or ethical restrictions.

Declarations

Competing interests The authors declare that they have no conflict of interest.

Ethical Approval and Consent to participate Not applicable.

Consent for publication Not applicable.

References

1. Wang, K., M. Wang, X. Liao, S. Gao, J. Hua, X. Wu, et al. 2022. Locally organised and activated Fth1(hi) neutrophils aggravate inflammation of acute lung injury in an IL-10-dependent manner. *Nature Communications* 13: 7703.
2. Xu, H., S. Sheng, W. Luo, X. Xu, and Z. Zhang. 2023. Acute respiratory distress syndrome heterogeneity and the septic ARDS subgroup. *Frontiers in Immunology* 14: 1277161.
3. Qu, L., Y. Li, C. Chen, T. Yin, Q. Fang, Y. Zhao, et al. 2022. Caveolin-1 identified as a key mediator of acute lung injury using bioinformatics and functional research. *Cell Death & Disease* 13: 686.
4. Kim, Y., C.R. Bae, D. Kim, H. Kim, S. Lee, H. Zhang, et al. 2023. Efficacy of CU06-1004 via regulation of inflammation and endothelial permeability in LPS-induced acute lung injury. *Journal of Inflammation (London)* 20: 13.
5. Liu, C., K. Xiao, and L. Xie. 2022. Advances in the use of exosomes for the treatment of ALI/ARDS. *Frontiers in Immunology* 13: 971189.
6. Land, W.G. 2021. Role of DAMPs in respiratory virus-induced acute respiratory distress syndrome-with a preliminary reference to SARS-CoV-2 pneumonia. *Genes and Immunity* 22: 141–160.
7. Fan, E.K.Y., and J. Fan. 2018. Regulation of alveolar macrophage death in acute lung inflammation. *Respiratory Research* 19: 50.
8. Zoulikha, M., Q. Xiao, G.F. Boafo, M.A. Sallam, Z. Chen, and W. He. 2022. Pulmonary delivery of siRNA against acute lung injury/acute respiratory distress syndrome. *Acta Pharm Sin B* 12: 600–620.
9. Fajgenbaum, D.C., and C.H. June. 2020. Cytokine Storm. *New England Journal of Medicine* 383: 2255–2273.
10. Li, W., D. Li, Y. Chen, H. Abudou, H. Wang, J. Cai, et al. 2022. Classic Signaling Pathways in Alveolar Injury and Repair Involved in Sepsis-Induced ALI/ARDS: New Research Progress and Prospect. *Disease Markers* 2022: 6362344.
11. Cockram, P.E., M. Kist, S. Prakash, S.H. Chen, I.E. Wertz, and D. Vucic. 2021. Ubiquitination in the regulation of inflammatory cell death and cancer. *Cell Death and Differentiation* 28: 591–605.
12. Snyder, N.A., and G.M. Silva. 2021. Deubiquitinating enzymes (DUBs): Regulation, homeostasis, and oxidative stress response. *Journal of Biological Chemistry* 297: 101077.
13. Schubert, A.F., J.V. Nguyen, T.G. Franklin, P.P. Geurink, C.G. Roberts, D.J. Sanderson, et al. 2020. Identification and characterization of diverse OTU deubiquitinases in bacteria. *EMBO Journal* 39: e105127.
14. Koschel, J., G. Nishanth, S. Just, K. Harit, A. Kroger, M. Deckert, et al. 2021. OTUB1 prevents lethal hepatocyte necroptosis through stabilization of c-IAP1 during murine liver inflammation. *Cell Death and Differentiation* 28: 2257–2275.
15. Wu, B., L. Qiang, Y. Zhang, Y. Fu, M. Zhao, Z. Lei, et al. 2022. The deubiquitinase OTUD1 inhibits colonic inflammation by suppressing RIPK1-mediated NF-kappaB signaling. *Cellular & Molecular Immunology* 19: 276–289.
16. Schunke, H., U. Gobel, I. Dikic, and M. Pasparakis. 2021. OTULIN inhibits RIPK1-mediated keratinocyte necroptosis to prevent skin inflammation in mice. *Nature Communications* 12: 5912.
17. Song, J., T. Liu, Y. Yin, W. Zhao, Z. Lin, Y. Yin, et al. 2021. The deubiquitinase OTUD1 enhances iron transport and potentiates host antitumor immunity. *EMBO Reports* 22: e51162.
18. Zhu, W., W. Luo, J. Han, Q. Zhang, L. Ji, A.V. Samorodov, et al. 2023. Schisandrin B protects against LPS-induced inflammatory lung injury by targeting MyD88. *Phytomedicine* 108: 154489.
19. Zhu, W., M. Wang, L. Jin, B. Yang, B. Bai, R.N. Mutsinze, et al. 2023. Licochalcone A protects against LPS-induced inflammation and acute lung injury by directly binding with myeloid differentiation factor 2 (MD2). *British Journal of Pharmacology* 180: 1114–1131.
20. Yang, Y., T. Ma, J. Zhang, Y. Tang, M. Tang, C. Zou, et al. 2023. An integrated multi-omics analysis of identifies distinct molecular characteristics in pulmonary infections of Pseudomonas aeruginosa. *PLoS Pathogens* 19: e1011570.
21. Zheng, X., J. Guo, C. Cao, T. Qin, Y. Zhao, X. Song, et al. 2022. Time-Course Transcriptome Analysis of Lungs From Mice Infected With Hypervirulent Klebsiella pneumoniae via Aerosolized Intratracheal Inoculation. *Frontiers in Cellular and Infection Microbiology* 12: 833080.
22. Wu, D.Q., H.B. Wu, M. Zhang, and J.A. Wang. 2017. Effects of Zinc Finger Protein A20 on Lipopolysaccharide (LPS)-Induced Pulmonary Inflammation/Anti-Inflammatory Mediators in an Acute Lung Injury/Acute Respiratory Distress Syndrome Rat Model. *Medical Science Monitor* 23: 3536–3545.
23. Jang, J.H., H. Kim, I.Y. Jung, J.H. and Cho. 2021. A20 Inhibits LPS-induced inflammation by regulating TRAF6 polyubiquitination in rainbow trout. *International Journal of Molecular Sciences* 22: 9801.
24. Oikawa, D., M. Gi, H. Kosako, K. Shimizu, H. Takahashi, M. Shiota, et al. 2022. OTUD1 deubiquitinase regulates NF-kappaB- and KEAP1-mediated inflammatory responses and reactive oxygen species-associated cell death pathways. *Cell Death & Disease* 13: 694.
25. Le, J., E. Perez, L. Nemzow, and F. Gong. 2019. Role of deubiquitinases in DNA damage response. *DNA Repair (Amst)* 76: 89–98.
26. Vdovin, A., T. Jelinek, D. Zihala, T. Sevcikova, M. Durech, H. Sahinbegovic, et al. 2022. The deubiquitinase OTUD1 regulates immunoglobulin production and proteasome inhibitor sensitivity in multiple myeloma. *Nature Communications* 13: 6820.
27. Lu, D., J. Song, Y. Sun, F. Qi, L. Liu, Y. Jin, et al. 2018. Mutations of deubiquitinase OTUD1 are associated with autoimmune disorders. *Journal of Autoimmunity* 94: 156–165.
28. Zheng, S., Y. Li, X. Song, M. Wu, L. Yu, G. Huang, et al. 2023. OTUD1 ameliorates cerebral ischemic injury through inhibiting inflammation by disrupting K63-linked deubiquitination of RIP2. *Journal of Neuroinflammation* 20: 281.
29. Chen, X., H. Zhang, X. Wang, Z. Shao, Y. Li, G. Zhao, et al. 2021. OTUD1 Regulates Antifungal Innate Immunity through Deubiquitination of CARD9. *The Journal of Immunology* 206: 1832–1843.
30. Wang, M., X. Han, T. Yu, M. Wang, W. Luo, C. Zou, et al. 2023. OTUD1 promotes pathological cardiac remodeling and heart failure by targeting STAT3 in cardiomyocytes. *Theranostics* 13: 2263–2280.
31. Karlsson, M., C. Zhang, L. Mear, W. Zhong, A. Digre, B. Katona, et al. 2021. A single-cell type transcriptomics map of human tissues. *Science Advances* 7: eabh2169.
32. Rowinsky, E.K., A. Paner, J.G. Berdeja, C. Paba-Prada, P. Venugopal, K. Porkka, et al. 2020. Phase 1 study of the protein

deubiquitinase inhibitor VLX1570 in patients with relapsed and/or refractory multiple myeloma. *Investigational New Drugs* 38: 1448–1453.
33. Jiang, L., Y. Sun, J. Wang, Q. He, X. Chen, X. Lan, et al. 2019. Proteasomal cysteine deubiquitinase inhibitor b-AP15 suppresses migration and induces apoptosis in diffuse large B cell lymphoma. *Journal of Experimental & Clinical Cancer Research* 38: 453.
34. Rut, W., M. Zmudzinski, S.J. Snipas, M. Bekes, T.T. Huang, and M. Drag. 2020. Engineered unnatural ubiquitin for optimal detection of deubiquitinating enzymes. *Chemical Science* 11: 6058–6069.
35. Han, J., Y. Tian, L. Yu, Q. Zhang, X. Xu, Y. Zhang, et al. 2020. Discovery of novel USP8 inhibitors via Ubiquitin-Rho-110 fluorometric assay based high throughput screening. *Bioorganic Chemistry* 101: 103962.
36. Cho, J., J. Park, E.E. Kim, and E.J. Song. 2020. Assay systems for profiling deubiquitinating activity. *International Journal of Molecular Sciences* 21: 5638.